Flow Surge Computation for Dynamic River Breakup

M. G. Ferrick and S. T. Hunnewell

USA Cold Regions Research and Engineering Laboratory

Hanover, NH 03755-1290

(603) 646-4100

Introduction

The forces applied to a river ice cover by the flowing water can cause ice breakup. In a "dynamic" breakup both the ice motion and the river flow exhibit large and rapid changes with time. As the ice cover begins to move downstream during breakup, the resistance to flow decreases, resulting in the development of a river surge. The flow velocity, depth and discharge at each point along the front of the surge are greater than those at the same locations prior to the ice motion. During periods of ice motion, the river flow records that are developed from river stage alone can be grossly inaccurate. Also, the ability to successfully model dynamic breakup depends on the representation of the unsteady flow conditions that accompany breakup. Attempts at modeling frequently suffer from a lack of data to correctly specify the flow boundary conditions or to verify the model results.

Ferrick et al. (1991) analyzed the ice motion over a 300-s period beginning with the initial movement during a controlled dynamic breakup of the Connecticut River. As a first approximation they considered the flow parameters as constant at their mean values for this period. In this paper we will consider this same event and time period, but focus on the coupling between the ice motion and the surging response of the river flow. Included in the development of the coupled equations is a generalized equation for composite channel roughness that accounts for the motion of the ice cover. This equation contains an unknown parameter that is specified with the condition that the

hydraulic radius of the composite channel should be independent of the relative roughnesses of the ice and the bed. Then, with river stage, ice velocity, and other basic flow and channel parameters known, we obtain the resistance to ice motion, hydraulic radius, composite roughness, discharge and flow velocity with time. At present there are no methods available to obtain critical flow parameters during a dynamic breakup or following the release of an ice jam. The primary advantage of the variable flow analysis against one based on the mean flow is the ability to quantify the flow surge. The effect of ice roughness on surge development is shown by keeping all other parameters constant.

River Flow Response to Ice Motion

In this section we develop the equations that couple the ice motion to the flow surge. The river is idealized as a wide rectangular channel with constant width B. The ice cover is initially stationary at the ice velocity measurement location until the arrival of the breaking front. We consider the river as a composite with a portion of the depth dominated by ice resistance and the remainder dominated by bed resistance. We write Manning and continuity equations for each portion of the channel depth and for the composite. The bed and the ice are each assumed to have known Manning roughness. When the breaking front arrives, the ice begins to accelerate. The hydraulic radius associated with the ice is a function of the relative velocity between the ice and the water, coupling the ice velocity to the

hydraulic equations. Closure of the system of coupled equations is obtained with an estimated energy gradient S_f from the measured data.

Ice velocity on the Connecticut River during a controlled dynamic breakup experiment was measured as a function of time by Ferrick et al. (1991) at a site 26 km downstream of the primary flow control dam. These data were fitted with a polynomial as

$$v_I(\tilde{t}) = a_o + a_1\tilde{t} + a_2\tilde{t}^2 + \ldots + a_5\tilde{t}^5 \qquad (1)$$

where time, $\tilde{t}$, was measured from the arrival of the breaking front and $a_o \approx 0$ because $v_I(0) = 0$. The river stage at this site was also measured with time.

Manning's equation can be written for each portion of the channel and for the composite as

$$Q_I = B\, Y_I \left[\frac{R_I^{2/3}\, S_f^{1/2}}{n_I}\right]$$

$$Q_B = B\, Y_B \left[\frac{R_B^{2/3}\, S_f^{1/2}}{n_B}\right] \qquad (2)$$

$$Q = B\, Y \left[\frac{R^{2/3}\, S_f^{1/2}}{n_c}\right]$$

where

Q_I, Q_B, Q = discharge associated with the ice, the bed, and the composite, respectively,

Y_I, Y_B, Y = flow depths,

R_I, R_B, R = hydraulic radii,

n_I, n_B, n_c = Manning's roughnesses.

The discharges and depths of the composite section are related as

$$Q = Q_I + Q_B \tag{3}$$

$$Y = Y_I + Y_B \tag{4}$$

The definition of the hydraulic radius for a wide channel yields

$$R_I = A_I/P_I = BY_I/B = Y_I$$

$$R_B = A_B/P_B = BY_B/B = Y_B \tag{5}$$

where A and P are cross-sectional area and wetted perimeter, respectively. Then, from (2), (3) and (5) we obtain

$$\frac{YR^{2/3}}{n_c} = \frac{Y_I^{5/3}}{n_I} + \frac{Y_B^{5/3}}{n_B} \tag{6}$$

The continuity equation for the composite section is

$$Q = B\ Y\ V_w \tag{7}$$

As ice motion begins, the portion of the discharge associated with the ice Q_I diminishes. The limiting conditions are when $V_I = V_w$, then $Q_I = 0$, and when $V_I = 0$, then the discharge split of the river section is determined by the relative roughnesses of the bed and the ice cover. For the part of the section dominated by the ice resistance, the continuity equation is

$$Q_I = B\, Y_I\, (V_w - V_I) \tag{8}$$

Then using (3), (7) and (8), we obtain the continuity equation for the bed discharge as

$$Q_B = B\, Y_B \left[V_w + \frac{Y_I}{Y_B} V_I\right] \tag{9}$$

In rivers where dynamic breakup occurs, the average bed slope S_o is generally greater than 0.0001. Ferrick (1985) showed that in this range of S_o the flow inertia makes a negligible contribution to momentum. On wave fronts where breakup occurs the inertia terms of the momentum equation have opposite signs, and their sum is smaller than the absolute value of each term. Then with small local inflows relative to the river flow, the momentum equation for prismatic channels is (Ferrick et al., 1984)

$$S_f = S_o - \frac{\partial Y}{\partial x} \tag{10}$$

where x is distance along the river. If we assume that wave diffusion over short distances is not significant, (10) can be rewritten in a form that can be evaluated with data at a point

$$S_f \approx S_o + \frac{1}{c}\frac{\partial Y}{\partial t} \tag{11}$$

where $c = \frac{3}{2} V_w$, the speed of a kinematic wave, and t is time.

Composite Channel Roughness

Our development of an equation for composite channel roughness begins with a temporary assumption of $V_I = 0$. Then, (8) and (9) together with (2) provide

$$\frac{V_w}{S_f^{1/2}} = \frac{Y_I^{2/3}}{n_I} = \frac{Y_B^{2/3}}{n_B} = \frac{R^{2/3}}{n_c} \tag{12}$$

and

$$\left(\frac{Y_I}{Y_B}\right)^{2/3} = \frac{n_I}{n_B} \tag{13}$$

Noting that $R = Y/2$ when $V_I = 0$, we can be rearrange (6) using (13) to obtain the Belokon-Sabaneev formula for composite Manning's roughness

$$n_c = \left[\frac{n_B^{3/2} + n_I^{3/2}}{2}\right]^{2/3} \tag{14}$$

More generally, $V_I \neq 0$ and the equation for composite roughness must take the ice motion into account.

The constraints on the composite roughness relationship are that it must simplify to (14) when $V_I = 0$, and yield $n_c = n_B$ for the condition $V_I = V_w$. If the bed and ice roughnesses are equal, the composite roughness must have this value for any V_w and V_I. In all cases, n_c is confined to a range with limits of n_B and n_I. A generalized equation for composite roughness that satisfies all of these constraints, assuming $V_I < V_w$, is

$$n_c = \left[\frac{n_B^{3/2} + n_I^{3/2} \left(1 - \frac{V_I}{V_w} \right)^m}{1 + \left(1 - \frac{V_I}{V_w} \right)^m} \right]^{2/3} \qquad (15)$$

where m is an arbitrary exponent > 0. The composite roughness given in (15) represents a weighted average of the bed and ice cover flow resistances.

Constraints that can be imposed to bound m follow from the requirement that $Y/2 \leq R \leq Y$. Rewriting (2) using (15) yields

$$R = \left(\frac{V_w n_c}{S_f^{1/2}} \right)^{3/2} = \left(\frac{V_w}{S_f^{1/2}} \right)^{3/2} \left\{ \frac{n_B^{3/2} + \left(1 - \frac{V_I}{V_w} \right)^m n_I^{3/2}}{1 + \left(1 - \frac{V_I}{V_w} \right)^m} \right\} \qquad (16)$$

Rough ice with $n_I > n_B$ is the condition that could yield $R < Y/2$, the lower limit. Imposing the lower limit on R requires

$$\left(1 - \frac{V_I}{V_w}\right)^m (n_I^{3/2} - A) \geq (A - n_B^{3/2}) \tag{17}$$

where

$$A = \frac{Y}{2}\left(\frac{S_f^{1/2}}{V_w}\right)^{3/2}$$

With (2), (5) and (8) we observe that

$$n_I^{3/2} = Y_I \left(\frac{S_f^{1/2}}{V_w - V_I}\right)^{3/2} \tag{18}$$

When $Y_I > \frac{Y}{2}$ and $V_I > 0$, then $n_I^{3/2} > A$ and (17) can be solved for m, yielding

$$m \leq \frac{\log\left[\frac{A - n_B^{3/2}}{n_I^{3/2} - A}\right]}{\log\left(1 - \frac{V_I}{V_w}\right)} \tag{19}$$

If the ice is smooth, Y_I is smaller than $\frac{Y}{2}$ and $n_I^{3/2} < A$. Then from (17) we again obtain (19), except that the inequality is reversed and the sign of the right hand side is also reversed.

Imposing the upper limit Y on R yields a constraint equation very similar to (17)

$$\left(1 - \frac{V_I}{V_w}\right)^m (n_I^{3/2} - A') \leq (A' - n_B^{3/2}) \tag{20}$$

with

$$A' = Y \left(\frac{S_f^{1/2}}{V_w}\right)^{3/2}$$

Combining (2), (5) and (9), we find that

$$n_B^{3/2} = Y_B \left(\frac{S_f^{1/2}}{V_w + \frac{Y_I}{Y_B} V_I}\right)^{3/2} \tag{21}$$

With $Y \geq Y_B$ and $V_I Y_I / Y_B \geq 0$, (20) and (21) indicate that $A' \geq n_B^{3/2}$. Then, for smooth ice or rough ice with $n_I^{3/2} < A'$, (20) is satisfied for any positive m. With very rough ice and peak flow velocity $n_I^{3/2} > A'$ may be possible, and then (20) yields the constraint

$$m \geq \frac{\log \left[\frac{A' - n_B^{3/2}}{n_I^{3/2} - A'}\right]}{\log \left(1 - \frac{V_I}{V_w}\right)} \tag{22}$$

Numerical Algorithm

Given the river width, the energy gradient, the total discharge and depth, and the ice and bed roughnesses immediately prior to the breaking front arrival and initial ice motion, the equations above specify the component discharges and depths, the flow velocity, composite roughness, and the hydraulic radius. We

will assume that both the bed and ice roughnesses are constant locally during the ice motion. However, in cases where the ice floes are rapidly reduced in size following the initial motion, the ice roughness may vary as a function of time. This function must then be estimated and available as input data.

Following the arrival of the breaking front, we calculate the ice velocity at any time $\tilde{t}$ using (1). From (2), (5) and (8) the depth Y_I is found as

$$Y_I = \left[\frac{(V_w - V_I)\, n_I}{S_f^{1/2}}\right]^{3/2} \tag{23}$$

and with (2), (5) and (9) we obtain

$$Y_B^{5/3} - \frac{n_B}{S_f^{1/2}} (V_w Y_B + V_I Y_I) = 0 \tag{24}$$

Netwon's method can be used to solve (24) for Y_B. With Y_I and Y_B the discharges can be found from (2), (7), (8) and (9). Equations (2) and (15) provide the hydraulic radius R of the composite section.

When the ice is moving, the equations given above for depth, discharge, energy gradient, hydraulic radius and composite roughness all depend on the water velocity V_w. Because V_w is also unknown, it is initially assumed as the value at the previous time, and an error ΔV_w is found as

$$\Delta V_w = V_w - \frac{Q}{BY} \tag{25}$$

For the next iteration, V_w is updated, $V_w = V_w + \Delta V_w$, and the process repeats until ΔV_w is sufficiently small, indicating a converged solution.

Ferrick et al. (1991) showed that ice convergence near the measurement site was minimal, and lumped all the ice motion resistance into a bank resistance term. Because we are analyzing the same case, this approach is again taken and the bank shear τ_b is obtained as

$$\tau_b = \frac{\rho g\, S_f B(R_I + t_I \rho_I/\rho) - (1 + C_m)\, m_I \frac{dV_I}{dt}}{2t_I} \tag{26}$$

where

g = acceleration due to gravity,

t_I = ice thickness,

m_I = $t_I B \rho_I$, the mass of ice in the control volume,

C_m = coefficient of apparent or added mass, and

ρ, ρ_I = density of water and ice, respectively.

The equation for ice acceleration dV_I/dt developed by Ferrick et al. (1991) is

$$\frac{dV_I(x,t)}{dt} = \left(1 - \frac{v_I(\tilde{t})}{C_b}\right) \frac{dv_I(\tilde{t})}{d\tilde{t}} \tag{27}$$

where the derivative of ice velocity is found from (1). With all parameters known at time t, the time variable parameters are updated and the calculation is repeated for time $(t + \Delta t)$.

Results

We will now examine the behavior of the proposed algorithm over a range of m values and consider the implications of each choice. The cases included in this comparison range from rough ice ($n_I/n_B = 1.4$) to smooth ice ($n_I/n_B = 0.71$). Our estimate of the relative roughness in the field is 0.83, which is included as one of the cases. The composite roughness prior to ice motion is the same in all cases. The amplitude of the hydraulic radius variation shown in Figure 1 increases for smooth ice and decreases for rough ice as m increases. The amplitude of the composite roughness variation given in Figure 2 increases with m for both rough and smooth ice. As m approaches zero the composite roughness approaches a constant, the value of which is given by the Belokon-Sabaneev equation.

The condition given by (19) imposes the restriction $m \leq 0.92$ to ensure $R \geq \frac{Y}{2}$. This limit was verified by a series of model runs where the rough ice case with $m \geq 1.0$ had an initial dip in R below $\frac{Y}{2}$ (Fig. 1). The composite hydraulic radius for a stationary ice cover is independent of the relative roughnesses of the ice and the bed. The experimentally determined value of $m = \frac{2}{3}$ yields R values for these data that are independent of the relative roughnesses throughout the ice motion. We will use $m = \frac{2}{3}$ for the remainder of the simulations.

The calculated flow velocity response to the ice motion is presented together with the ice velocity polynomial in Figure 3. These curves have the same basic shape, but the amplitude of the flow fluctuations are greatly reduced relative to those of the ice. The dramatic nature of the unsteady flow during the ice motion becomes clearer by observing the changes in discharge with time given in Figure 4. The discharge increased by almost 200 m^3/s in 90 s, and the bed and ice discharges are even more dynamic. The flow velocity and discharge comparisons of these variable flow conditions with those for the same case but having a constant flow velocity and depth at the mean values (Ferrick et al., 1991) are also presented in Figures 3 and 4. Though the ice and bed discharges are similar for variable flow and constant flow conditions, the composite discharge and flow velocity are very different. Flow velocity and discharge must vary with time for the flow surge to be quantified by the method presented.

The composite Manning's roughness near the measurement location does not change substantially when the flow velocity varies (Fig. 5). However, this difference would increase as $| n_B - n_I |$ increases. The hydraulic radius comparisons given in Figure 6 are similar to those for discharge. The variable flow calculation produces a greater minimum R_I than that for constant flow, indicating a larger residual flow resistance of the ice than would otherwise be expected. The hydraulic radius of the composite section changes much more dramatically when the flow varies, as would be expected. The bank stresses displayed in Figure 7 vary with both dimensionless breaking front speed $C_b/\bar{V}_w$

and variable or constant flow conditions. Bank stresses are larger in the constant or time variable flow case, depending on which has a higher instantaneous flow velocity, for all values of the breaking front speed. In each case the shape of the bank stress curves are similar, and for any time the magnitude of the stresses do not vary greatly.

In many cases of interest the ice roughness passing the measurement site may vary with time or may not be known precisely. As a result, the sensitivity of the results to this parameter have practical importance. Several simulations with variable flow conditions were made for different relative roughnesses of the ice cover and bed n_I/n_B. As this ratio increases the amplitude of the flow velocity response to the ice motion, shown in Figure 8, becomes progressively larger and the change is more dynamic. The surging response of the flow to the ice motion is shown in Figure 9 for the same range of relative roughness. The residual that remains following the abrupt decrease in Q_I increases with the ice roughness, as does the peak composite discharge Q. The rate of increase of the discharge following the breaking front arrival also increases with ice roughness, corresponding to more dynamic conditions. The large and rapidly varying surge following a sudden release of an ice jam is just an extension of these results.

The hydraulic radius of the ice R_I shown in Figure 10 decreases rapidly following the start of the ice motion, but does not approach zero. The residual R_I like that of Q_I increases with ice roughness. The composite hydraulic radius R is again

independent of the relative roughness. Composite ice roughness as a function of time is given in Figure 11 for the range of relative roughness. In each case the composite roughness is the same for the stationary ice cover. As the ice velocity increases, the composite roughness approaches the bed roughness. For all of these cases, the amplitude of the roughness change is small relative to the initial roughness. The amplitude of the oscillation in the bank stress in Figure 12 increased with dimensionless breaking front speed for all relative roughnesses n_I/n_B. Higher ice roughness produces increased shear forces and bank stresses throughout the period of motion.

Conclusions

The dynamic breakup of a river ice cover is generally accompanied by a surging river flow. Basic hydraulic relationships that couple the flow to the ice motion were developed to calculate the dynamic variables that characterize this surge and the resistance to ice motion, with a known discharge before breakup, bed roughness and ice roughness measurements, and breakup ice velocity and river stage data. As a part of this algorithm an equation for composite channel roughness was developed with a single free parameter. Bounds on this parameter were obtained by constraining the range of the hydraulic radius, and it was specified experimentally with the condition that R is independent of the relative roughnesses of the ice and the bed, whether the cover is at rest or in motion. Sensitivity of the computation to ice roughness was carefully studied because

it may not be known precisely, or may vary with time during the breakup. When all other parameters are the same, the breakup of rougher ice leads to more dynamic flow and ice motion conditions.

Acknowledgement

Nate Mulherin assisted in the development of the plots that are presented in this paper.

References

Ferrick, M.G., P. B. Weyrick and S.T. Hunnewell (1991) Analysis of river ice motion near a breaking front. Awaiting publication, Canadian Journal of Civil Engineering.

Ferrick, M.G. (1985) Analysis of river wave types, Water Resources Research, vol. 21, pp. 209-220.

Ferrick, M.G., J. Bilmes and S.E. Long (1984) Modeling rapidly varied flow in tailwaters, Water Resources Research, vol. 20, pp. 271-289.

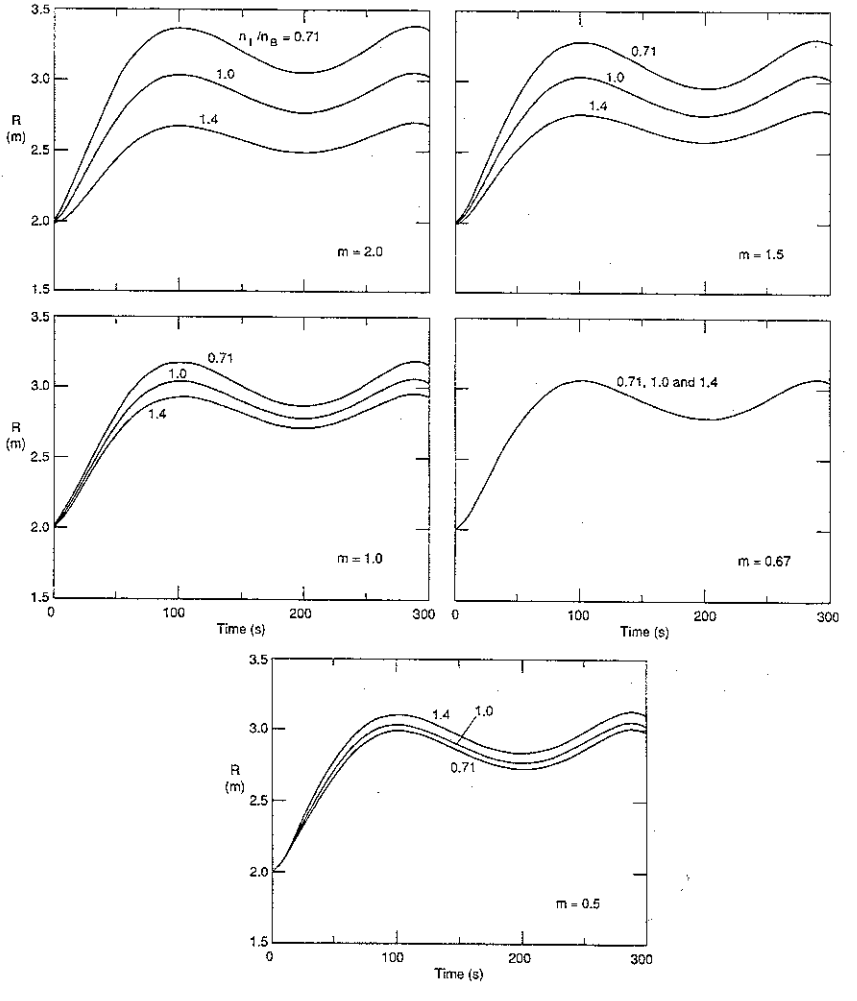

Figure 1. Hydraulic radius of the composite section as a function of time for ice roughness/bed roughness ratios of 1.4, 1.0 and 0.71 and selected m values between 0.5 and 2.0.

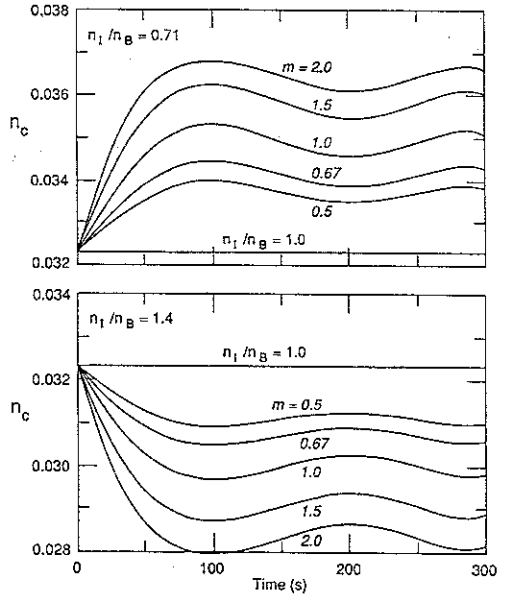

Figure 2. Manning's roughness of the composite section as a function of time for ice roughness/bed roughness ratios of 1.4, 1.0 and 0.71 and selected m values between 0.5 and 2.0.

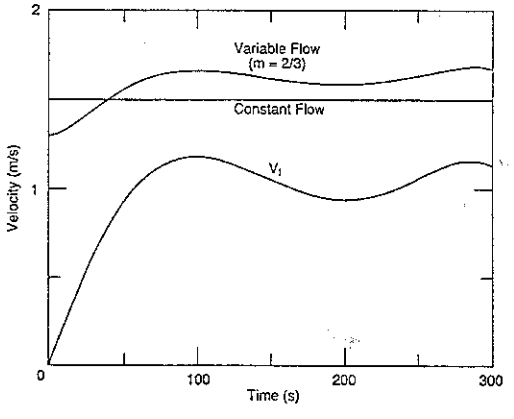

Figure 3. Ice velocity polynomial and flow velocity as a function of time for variable (n_I/n_B = 0.83) and constant flow conditions.

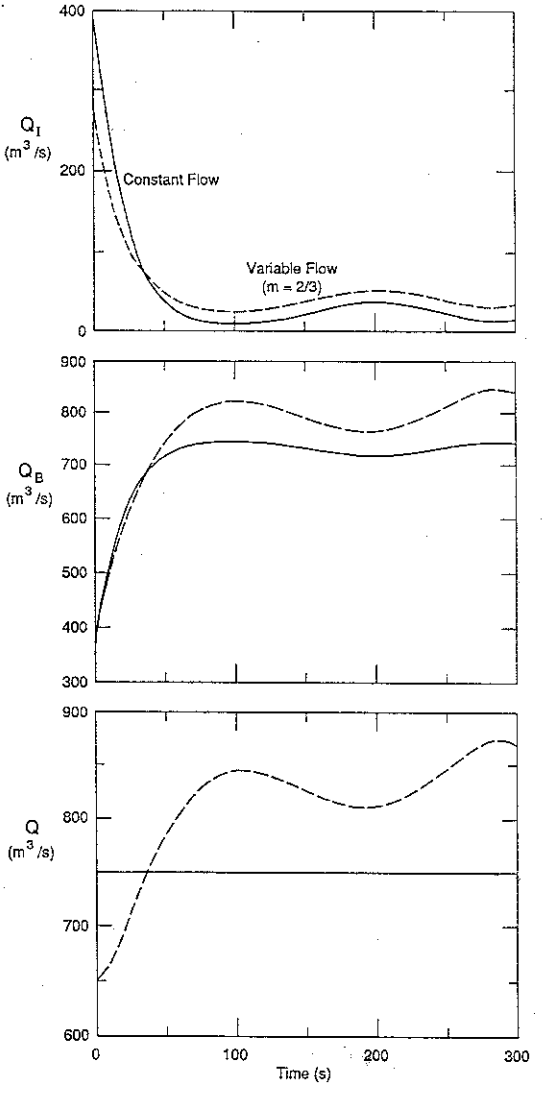

Figure 4. Discharge associated with the ice cover, the bed and the composite channel as a function of time for variable (n_I/n_B = 0.83) and constant flow conditions.

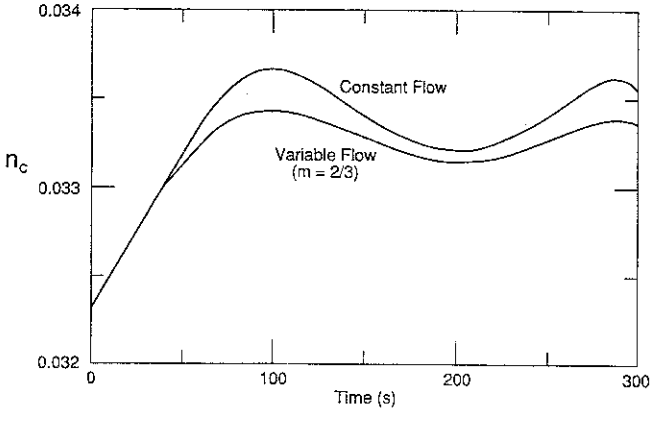

Figure 5. Composite Manning's roughness as a function of time for constant and variable flow conditions ($n_I/n_B = 0.83$).

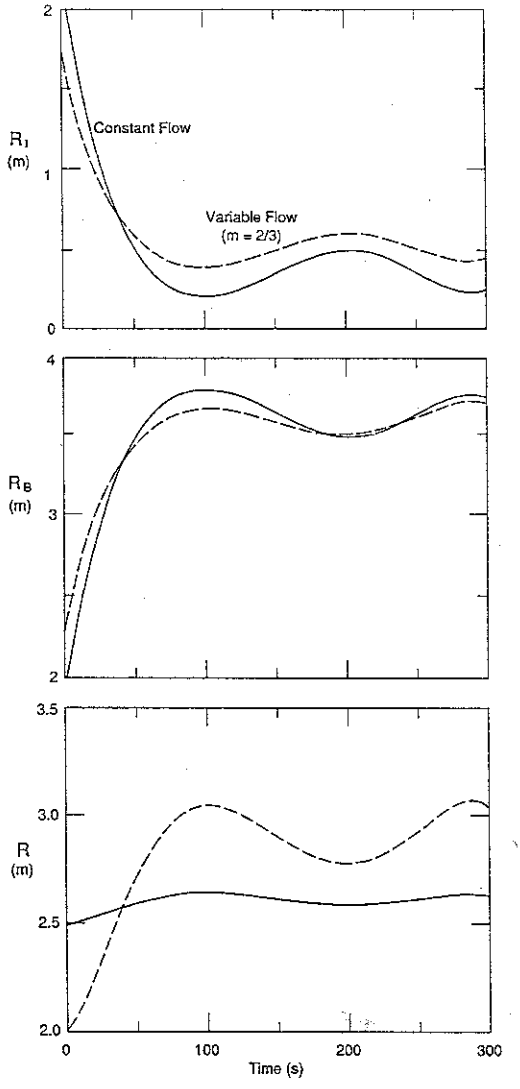

Figure 6. Hydraulic radius associated with the ice cover, the bed and the composite channel as a function of time for constant and variable flow conditions (n_I/n_B = 0.83).

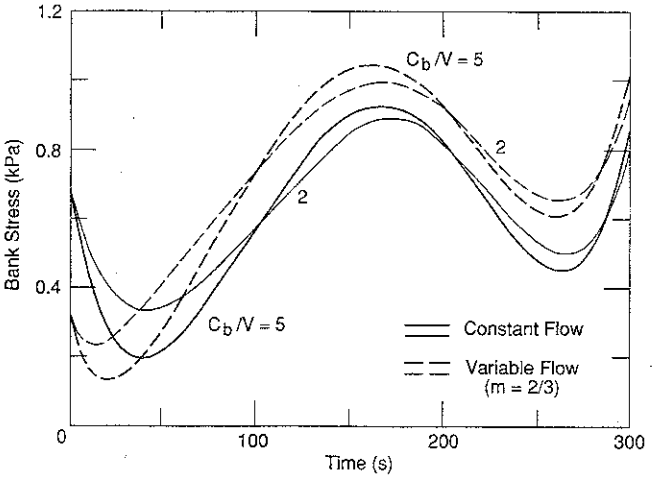

Figure 7. Bank stress as a function of time for constant and variable flow conditions ($n_I/n_B = 0.83$) and dimensionless breaking front speeds of 2 and 5.

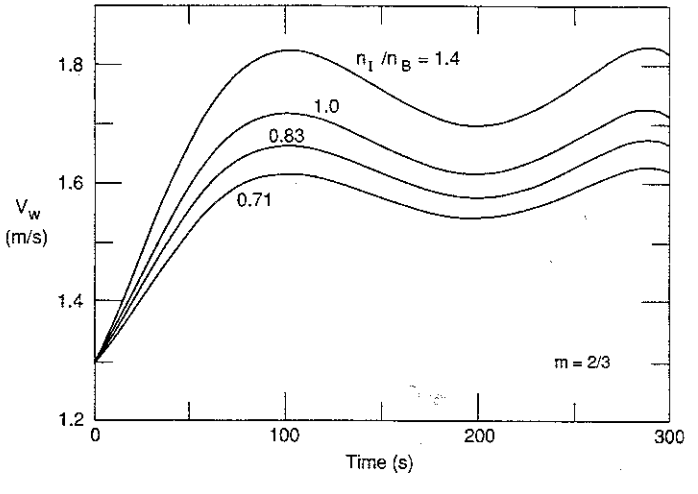

Figure 8. Flow velocity as a function of time for several values of the relative roughness of the ice cover and bed n_I/n_B.

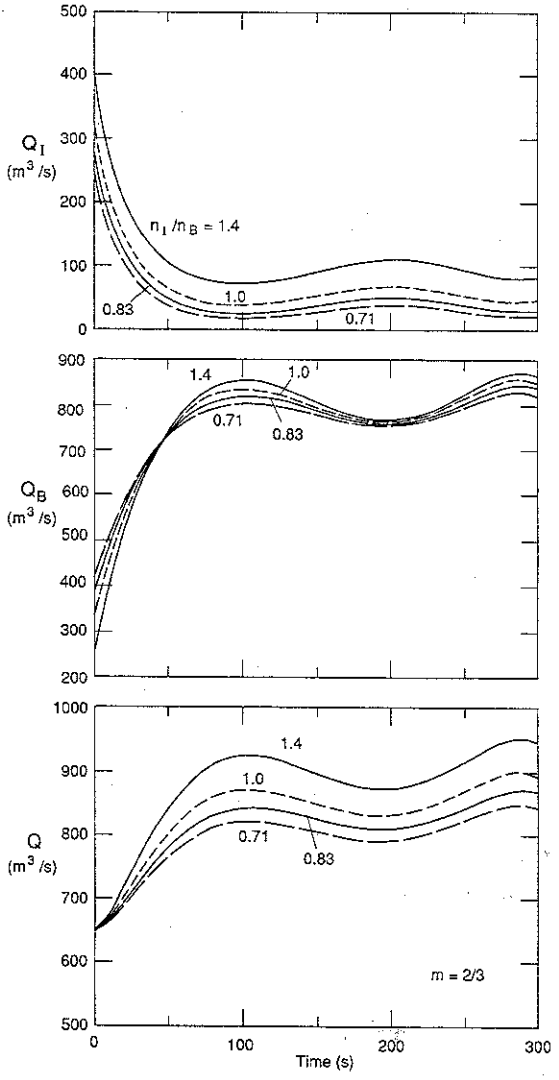

Figure 9. Discharge associated with the ice cover, the bed and the composite channel as a function of time for a range of relative roughnesses n_I/n_B.

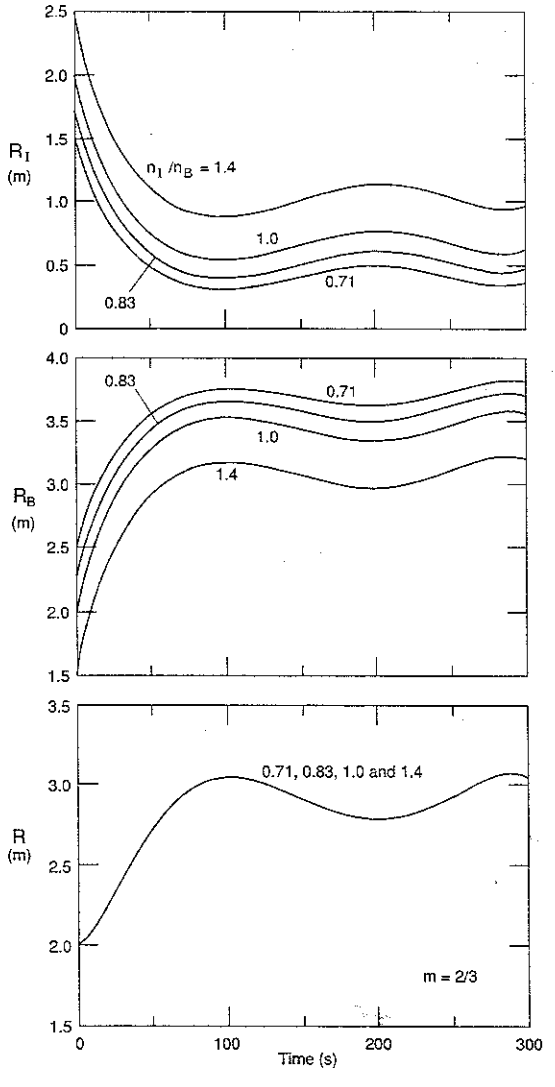

Figure 10. Hydraulic radius associated with the ice cover, the bed and the composite channel as a function of time for a range of relative roughnesses n_I/n_B.

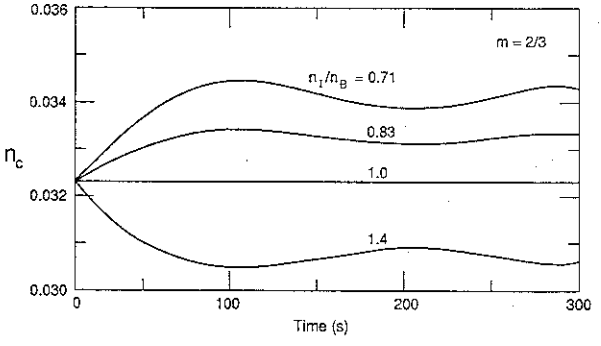

Figure 11. Manning's roughness of the composite section as a function of time for a range of relative roughnesses n_I/n_B.

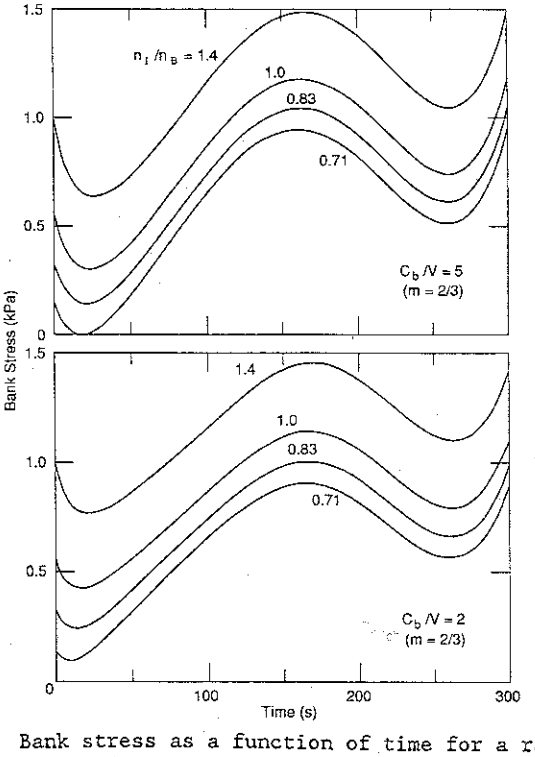

Figure 12. Bank stress as a function of time for a range of relative roughnesses n_I/n_B, and dimensionless breaking front speeds of 2 and 5.